DNA Base Detection Using a Single-Layer MoS_2

Amir Barati Farimani,[†] Kyoungmin Min,[†] and Narayana R. Aluru[*]

Department of Mechanical Science and Engineering, Beckman Institute for Advanced Science and Technology, University of Illinois at Urbana—Champaign, Urbana, Illinois 61801, United States. [†]These authors contributed equally to this work.

ABSTRACT Nanopore-based DNA sequencing has led to fast and high-resolution recognition and detection of DNA bases. Solid-state and biological nanopores have low signal-to-noise ratio (SNR) (< 10) and are generally too thick (> 5 nm) to be able to read at single-base resolution. A nanopore in graphene, a 2-D material with sub-nanometer thickness, has a SNR of ~3 under DNA ionic current. In this report, using atomistic and quantum simulations, we find that a single-layer MoS_2 is an extraordinary material (with a SNR > 15) for DNA sequencing by two competing technologies (*i.e.*, nanopore and nanochannel). A MoS_2 nanopore shows four distinct ionic current signals for single-nucleobase detection with low noise. In addition, a single-layer MoS_2 shows a characteristic change/response in the total density of states for each base. The band gap of MoS_2 is significantly changed compared to other nanomaterials (*e.g.*, graphene, h-BN, and silicon nanowire) when bases are placed on top of the pristine MoS_2 and armchair MoS_2 nanoribbon, thus making MoS_2 a promising material for base detection *via* transverse current tunneling measurement. MoS_2 nanopore benefits from a craftable pore architecture (combination of Mo and S atoms at the edge) which can be engineered to obtain the optimum sequencing signals.

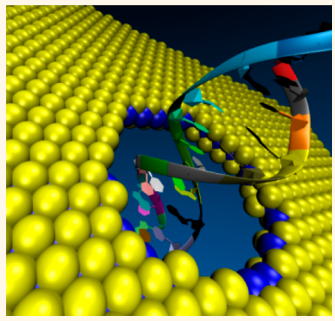

KEYWORDS: DNA · sequencing · nanopore · MoS_2 · electronic detection · MD · DFT

Nanopore-based DNA sequencing has opened up opportunities for fast and high-resolution recognition and detection of DNA bases (guanine (G), adenine (A), thymine (T), and cytosine (C)).[1−6] In these devices, a negatively charged DNA is driven through the nanopore along with other molecules such as water and ions.[2,5,7] DNA is electrophoretically[4] driven through a nanopore by an applied external electric field, and the ionic current through the nanopore is modulated during the DNA "translocation processes".[3,8] The change in the ionic current as the DNA molecule passes through the nanopore represents a direct reading of the DNA sequence.[3,5] The translocation occurs at speeds of about 10^7 bases per second, which is the sub-millisecond laboratory time scale.[9,10] Solid-state nanopores[11,12] and biological nanopores (*e.g.*, α-hemolysin)[13] have been extensively used for DNA sequencing.[1,2] In general, these membranes and pores are too thick (>5 nm) to be able to perform sequencing at single-base resolution.[11] Biological nanopores can be unstable, prone to be disassembled when biases higher than 1.0 V are applied, and can be quite sensitive to mechanical/thermal fluctuations.[2,14,15] To read the sequence of nucleotides in a DNA molecule, for example, a pore of nanometer thickness is required.[16] Graphene,[17] a 2-D material with a thickness of 0.34 nm, has conceptually been demonstrated for DNA translocation and sequencing.[9,14,16,18−20] The atomic-scale pore thickness can be used for DNA single-base detection.[18] In addition to ionic current blockade, transverse tunneling current can also be used for electronic base detection.[21−23] Sequencing by tunneling has already been accomplished using standard solid-state pores and break junctions.[24,25] It is notable that pristine graphene does not have a band gap,[17] which is not desirable for electronic base detection and field-effect transistors (FETs).[26] Engineering the band gap of graphene increases fabrication complexity[20,27] and either reduces the electronic mobility or requires high voltages which are beyond threshold voltages for DNA.[16] A single layer of MoS_2 has a direct band gap of 1.8 eV,[28] which can be used to construct interband tunnel FETs for sensing applications.[28] Recently, it has been shown that using hafnium oxide (HfO_2) as gate dielectric can enhance the single-layer MoS_2 mobility by about 200 times at room temperature, which makes

* Address correspondence to aluru@illinois.edu.

Received for review March 26, 2014 and accepted July 9, 2014.

Published online July 09, 2014
10.1021/nn5029295

it comparable to graphene nanoribbon mobility.[28] This finding makes MoS_2 highly preferable to graphene in terms of DNA electronic base sensing.

It has been shown that ionic current blockade signal shows noise for DNA translocation through a single-layer graphene nanopore.[16,29] The origin of this noise has been attributed to the atomic thickness of the pore. It is notable that a nanopore in a three-layer graphite structure, which has ~1 nm thickness, shows a better signal-to-noise ratio.[16,29,30] MoS_2 has a thickness of 1 nm, which makes it a superior material compared to graphene in terms of signal/noise intensity while maintaining its monolayer property.

Another issue with the graphene nanopore is that DNA sticks to the pore sides and surface during the translocation process.[14,16] Coexistence of bases on the surface and the pore sides will complicate the transverse tunneling current, making the nucleobase identification difficult. In addition, the stochastic motion of DNA through a nanopore generated due to the base adherence has under-defined interactions between the nanopore and the nucleobases.[9,16,31] Finding a substitute or a way to modify graphene for good sensing ability and nonsticky pore surface will be the challenge for the next generation DNA sequencing devices. Orientational fluctuations of nucleobases can give rise to overlapping current contributions from different bases, so it is advantageous to develop a device that can hold each base firmly while the base was being read.[15,31] The thickness of a single-layer MoS_2 nanopore combined with the ability to engineer atoms (molybdenum (Mo), sulfur (S), or both) exposed to DNA bases opens up opportunities for DNA sequencing. In a recent work, DNA is translocated through a single-layer MoS_2 and a signal-to-noise ratio (SNR) greater than 10 has been demonstrated.[32] In this paper, using molecular dynamics (MD) simulations, we demonstrate the translocation and sequencing of double-stranded DNA (dsDNA) through the MoS_2 nanopore with distinct ionic current blockade and low noise-to-signal ratio for each nucleobase. Furthermore, using density functional theory (DFT) simulation, we show that both MoS_2 nanopore and MoS_2 surface can be used for single DNA base detection. A comparison between graphene and the MoS_2 nanopore in terms of DNA adherence and pore architecture is also discussed.

RESULTS AND DISCUSSION

We performed MD simulations on translocation of dsDNA through a 2.3 nm diameter pore in a single-layer MoS_2 structure (Figure 1a,b). We used 2.3 nm pore size as prior studies for graphene nanopore have shown that a pore diameter of 2.3 nm is the smallest and most efficient pore size for the translocation of dsDNA[14]—specifically, this pore diameter shows better signatures of ionic current blockade for each DNA base and nucleotides.[19] Studies of the graphene nanopore also reveal that the pore size of ~2.3 nm would help to augment the transverse tunneling current due to the better mixing of the electronic cloud of carbon atoms and DNA bases. After equilibration (as described in the Methods section), electric field is applied in the *z*-direction. The translocation history of the DNA center of mass (COM) is registered for three biases of 2.1, 2.8, and 3.57 V. Complete electrophoresis of DNA for 2.1, 2.8, and 3.57 V takes 3.2, 0.3, and 0.18 ns, respectively. Generally, a bias of 100−600 mV is applied in experiments for DNA translocation through nanopores. Here, for tractable computational studies, we applied a higher bias. According to our simulation data (Supporting Information), for biases lower than 2.0 V, translocation is significantly hindered. Our estimates show that for biases of around 100 mV, the translocation time increases to microseconds. In all nanopore technologies, the high speed at which DNA is translocated through nanopores is very promising in ultrafast sequencing (1 base/μs); however, the measurement of small currents requires the bandwidth to be of MHz,[2] which limits the optimum sequencing speed. The red dashed line in Figure 1c represents the pore midline which is aligned along the *x*-axis. For a low bias of 2.1 V, DNA (COM) oscillates around the midline. Initially, when the dsDNA is located a few angstroms away from the pore mouth, we observed the transient flux of ions and water (Supporting Information) as the dsDNA approaches the pore entrance.

Due to the confinement in the pore, dsDNA acts like a pump and pushes ions and water molecules inside the pore. To calculate the residence time and translocation history of each base inside the pore, we tagged the atoms of each base when they were inside the pore. We counted the number of atoms of each base which occupied the pore at different time instances. Figure 2a shows the density of each base inside the pore (for a bias of 2.8 V). It is observed that A−T and C−G bases occupy the pore most of the time. At t = 250 ps, interestingly, only base A dominates the whole pore. Base T occupies the pore for t = 100−250 ps. We computed the ionic current blockade, $I(t)$, when the DNA passes through the pore. The ionic current through the nanopore is shown in Figure 2b. The computed ionic current in Figure 2b is in nanoampere range, which is in agreement with experiments.[32] We associate the bases, A, T, C, and G with the corresponding ionic current. At some time instances, two bases coexist in the pore and the associated ionic current is for both the bases combined. As shown in Figure 2b, the ionic current associated with the bases decreases as AT > G > T > CG > C. This result also accounts for orientation of bases in the pore, and we note that the effective blockade is higher for C and G bases compared to A and T (Supporting Information). We compared the noise in ionic current in graphene and MoS_2 nanopores by considering the same pore size and

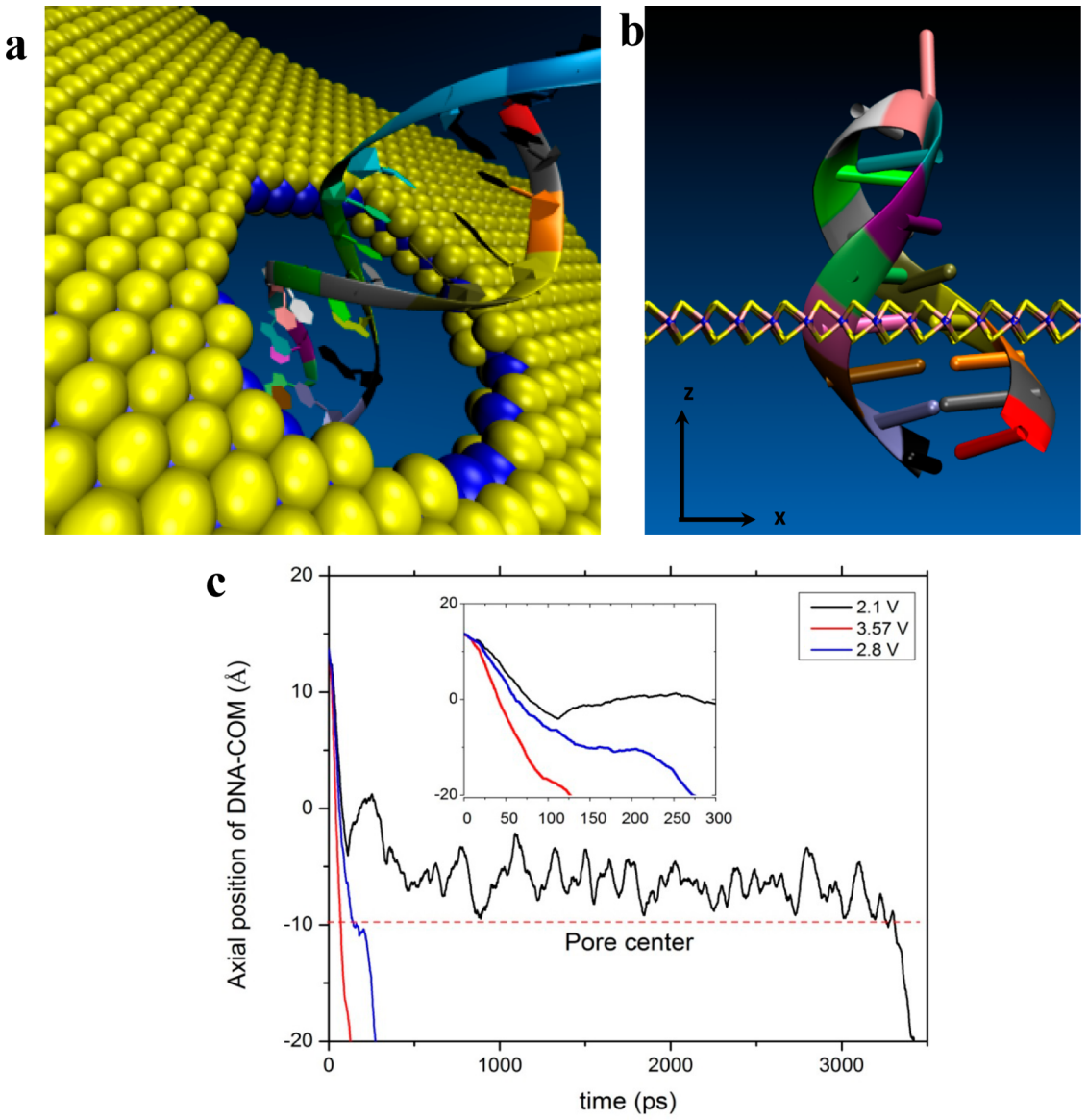

Figure 1. (a) DNA translocation through a MoS_2 nanopore. (b) DNA hairpin structure with the loop at the top (PDB code: 1ac7 taken from PDB.org) and the side view of MoS_2 fish-bone structure. (c) DNA translocation history for different biases; the red dashed line represents the center of the pore.

applied bias (Supporting Information). We found four distinct conductance states for the MoS_2 nanopore compared to graphene, which has only two conductance states. Graphene thickness is too small to capture the ionic current appropriately, and two conductance states are not enough to distinguish all the bases in the pore. For example, the chloride ion size (σ) is larger than the pore thickness (t) (σ = 0.41 nm compared to pore thickness of graphene, t = 0.34 nm), and the effective pore occupation length of each base is larger than the graphene pore thickness. The origin of more conduction states in the MoS_2 nanopore can be attributed to the architecture of the pore that contains both hydrophobic (S atoms) and hydrophilic (Mo atoms) sites. We computed the signal-to-noise ratio[33] of MoS_2 and graphene nanopores (Supporting Information). SNR for MoS_2 and graphene nanopore is 15.02 and 3.32, respectively. The SNR results are in agreement with the experiments suggesting that the SNR of DNA ionic current in a MoS_2 nanopore is higher than 10.[32] The noise generated in graphene is 4−5 times larger compared to MoS_2. The best SNR taken for any nanopore (biological and solid state) to our current knowledge[34] is around 10, which is lower than MoS_2 SNR. In addition, the noise is significantly higher in the case of graphene. In the case of the MoS_2 nanopore, the thickness of 1 nm combined with alternative arrangement of pore atoms (Mo/S) with hydrophobic−hydrophilic−hydrophobic architecture makes MoS_2 amenable for ionic current measurements with lower noise. Our findings can pave the way toward efficient DNA sequencing by ionic current measurements.

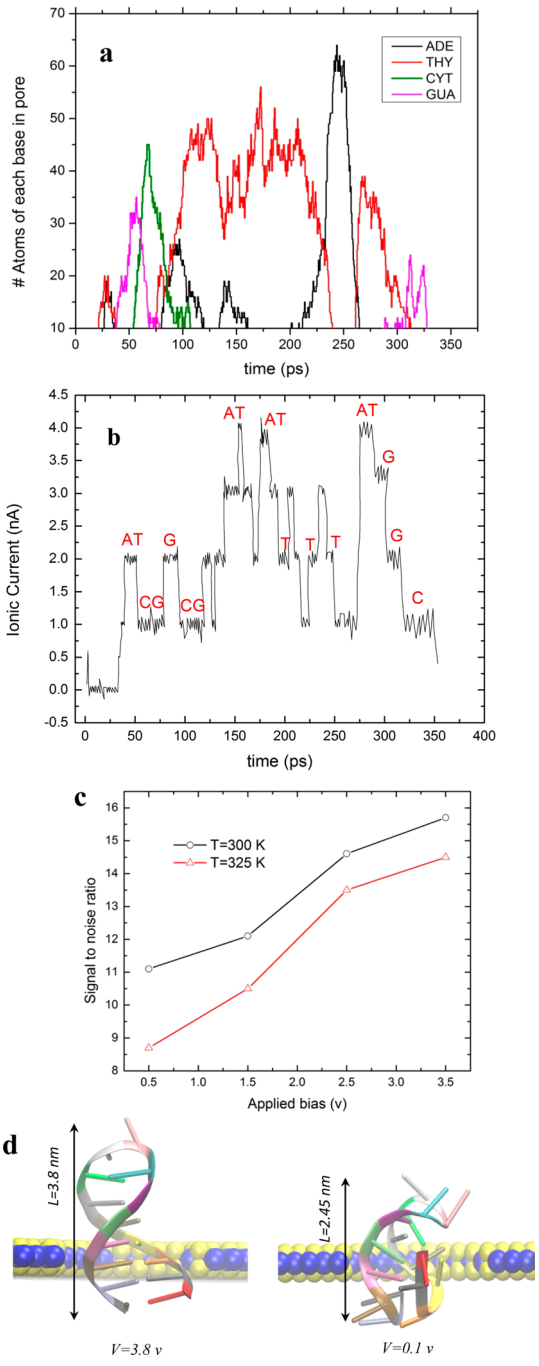

Figure 2. (a) Passage of bases (A, C, G, and T) through the MoS_2 nanopore and the residence time of each base inside the pore. (b) Ionic current for different bases and combination of CG or AT bases. (c) Signal-to-noise ratio of MoS_2 nanopore for different biases and temperatures, T = 300 K and T = 325 K. (d) dsDNA modalities for two different applied voltages. The average length of dsDNA during translocation is shown for the two cases. dsDNA knots inside the pore (right); electrophoretic forces are not strong enough to stretch and translocate dsDNA.

Thermal Fluctuations and DNA Modalities. To understand the effect of thermal fluctuations on the quality of the signal computed, we analyzed the effect of temperature on the noise generated in the pore. In all the pores, the translocation forces, which are electrostatic, compete with the drag forces in the nanopore.[35] The drag forces arise from the van der Waals interactions with the pore atoms. We changed the strength of the applied bias and temperature to examine its effect on the SNR (see Supporting Information for the calculation of SNR). Figure 2c shows that, as we increase the applied bias, SNR increases. Also, as we increase the temperature from T = 300 to 325 K, SNR decreases for all the applied biases. The decrease in SNR with increase in temperature is due to the increase in thermal vibration which gives rise to a larger stochastic motion of the bases in the pore. The root mean square displacement (RMSD) calculation of dsDNA in the MoS_2 nanopore (in the absence of applied bias) reveals a higher DNA fluctuation (RMSD = 3.65 Å) for T = 325 K compared to T = 300 K (RMSD = 2.93 Å). The higher rmsd indicates a higher frequency of bases entering and exiting the pore. This can be further confirmed by the comparison with $I_{noise,rms}$ (Supporting Information). $I_{noise,rms}$ is higher for T = 325 K compared to T = 300 K. From Figure 2c, it can be inferred that higher biases can enhance the SNR which can be attributed to stretching of the dsDNA.

We measured the time-averaged maximum length of dsDNA in the presence of an applied bias, and we observed that the stretching of the dsDNA increases with the bias (Figure 2d). The snapshots of dsDNA modalities for V = 0.1 and 3.0 V reveal that dsDNA knotting occurs frequently in lower biases in the nanopore, giving rise to a higher noise due to presence of a multibase in the nanopore (Figure 2d).

Stickiness of the Pores. One of the other challenges posed by DNA translocation through a graphene nanopore is the sticking behavior of DNA to the pore internal carbons and the surface of graphene.[14,16] We performed MD simulations for both graphene and the MoS_2 nanopore in order to compare their stickiness (to DNA) behavior (Supporting Information). Surprisingly, DNA did not adhere to MoS_2 in contrast to graphene where significant stickiness is observed (see supporting video, adherence). Liu *et al.* also found, by experiments, that DNA does not stick to the surface of MoS_2.[32] The architecture of the MoS_2 pore has Mo atoms which are strong hydrophilic sites. DNA is a hydrophobic structure, so it does not like to adhere to Mo sites. We performed MD simulations on two types of pore structures (Mo exposed only and S exposed only). Our observations suggest that having more Mo exposed in the pore would decrease the sticking of atoms to the pore sides and surface. These results open up opportunities for engineering the pore architecture for optimized DNA translocation through MoS_2.

DFT Results. *Bases in the MoS_2 Nanopore.* To demonstrate the significance of using MoS_2 as a DNA FET[36,37] for nucleobase detection (see Figure 3a for proposed architecture), we computed the electronic structure changes induced due to the presence of DNA bases inside the nanopore using DFT.

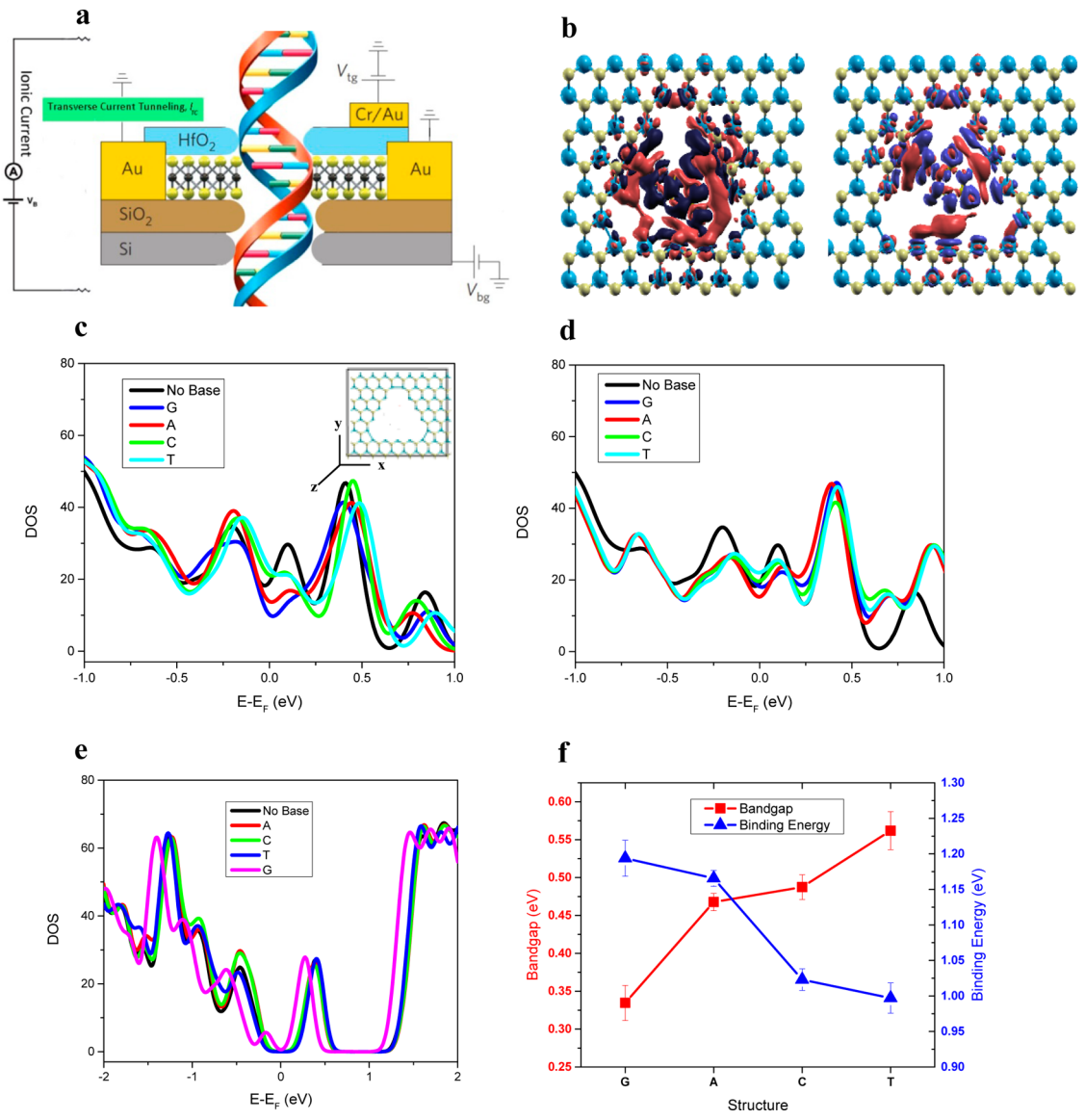

Figure 3. (a) Schematic view of a potential DNA sensing device. (b) Three-dimensional electronic charge density rearrangement ($\Delta\rho$) (red and blue isosurfaces represent charge accumulation and depletion, respectively; isosurface level is set at 0.0004 Å^{-3}) when porous (Mo-terminated) MoS_2 interacting with G (left) and T (right). Total DOS of each base when placed (c) horizontally (inset: molecular snapshot of Mo-only edge) and (d) at 45° angle in porous (Mo-terminated) MoS_2. (e) Total DOS and (f) band gap (left axis) and binding energy (right axis) of a pristine single-layer AMNR with each DNA base placed on the top of AMNR.

In MoS_2 nanopores, the atoms exposed to DNA bases can be engineered with three possible configurations: Mo-terminated, S-terminated, and both Mo- and S-terminated edge. We first constructed a MoS_2 nanopore with Mo termination. The charge density rearrangement ($\Delta\rho$) in the nanopore (Mo-terminated) due to the interaction between MoS_2 and DNA bases is shown in Figure 3b. It indicates that there are more overlapped electron clouds when G is inside the nanopore compared to T. This result suggests that base G will give rise to a higher conductance if bias is applied to the device.

To further investigate the effect of DNA bases (inside the pore) on MoS_2, the total density of states (DOS) was obtained as shown in Figure 3c, and it shows that the Mo-terminated pore induces finite states around the Fermi level.[38] Each base is placed in a planar configuration (θ = 0 and α = 0, Supporting Information) in the nanopore. The shape of the total DOS is significantly changed around the Fermi level, as shown in Figure 3c, which indicates a strong interaction of the bases with MoS_2. Each base shows a different response, and G and A bases interact stronger than the other two bases (G > A > C > T), supported by the binding energy calculation as shown in Table 1. This can be further confirmed when the DNA bases are placed at an orientation that is the most probable orientation (θ = 40−52°) obtained from MD simulations (Supporting Information). Similar to the case when the bases are placed horizontally, each DOS curve shows a distinct response for DNA base interaction

with the MoS_2 nanopore, and binding energy calculations also confirm this result as shown in Figure 3d and Table 1.

Next, we also constructed two other configurations: S-terminated nanopore and both Mo- and S-terminated nanopore. As shown in the Supporting Information, it should be noted that there is no distinct change in the total DOS when each base is placed horizontally, and the overall response is the same for all the bases. These results suggest that Mo atoms interact strongly with DNA bases compared to the S atoms, and Mo-terminated nanopores can potentially differentiate each base. This finding can be potentially used for the construction of a DNA FET sensor for electronic detection of each base.

Interaction of Armchair MoS_2 Nanoribbon (AMNR) with DNA Bases. To further investigate the potential application of a single-layer MoS_2 as a DNA sensing device in a nanochannel configuration, we studied the interaction of DNA bases with a pristine armchair MoS_2 nanoribbon (AMNR) without any pore or defects (device architecture and AMNR setup are shown in Supporting Information). A similar concept has been proposed by Min *et al.* using a graphene nanoribbon (GNR), where a unique response of GNR to DNA bases has been demonstrated.[9] Unlike the zigzag MoS_2 nanoribbon, which is a metal, AMNR exhibits a finite energy gap of 0.5349 eV that makes it amenable as a sensor.[39,40] We performed DFT simulations by placing each nucleobase on top of AMNR in a planar configuration (Supporting Information). A total of 10 different configurations for each structure are considered, and the average band gap is obtained. As shown in Figure 3e, the total DOS of AMNR shows a characteristic response in the presence of each base. The band gap of each system is highly affected due to the presence of bases. Base G most significantly affects AMNR and gives rise to a reduction in band gap by 0.2 eV compared to pristine AMNR. Unlike other bases, base T slightly opens the band gap of AMNR by 0.02 eV. The change in band gap is highest with base G and lowest with T and follows the order G > A > C > T (Figure 3f), which is the same order obtained for the MoS_2 nanopore (Mo-terminated) case. Interestingly, this order is also observed for the interaction of pristine graphene with DNA bases.[41,42] The binding energy calculation further confirms this result, which shows a larger value for the case with higher change in band gap

TABLE 1. Binding Energy Calculation between MoS_2 Terminated with Mo Only and Each Base

base orientation	bases	binding energy (eV)
horizontal	A	3.563
	C	3.246
	G	4.306
	T	1.603
angle	A	2.587
	C	2.153
	G	2.873
	T	1.755

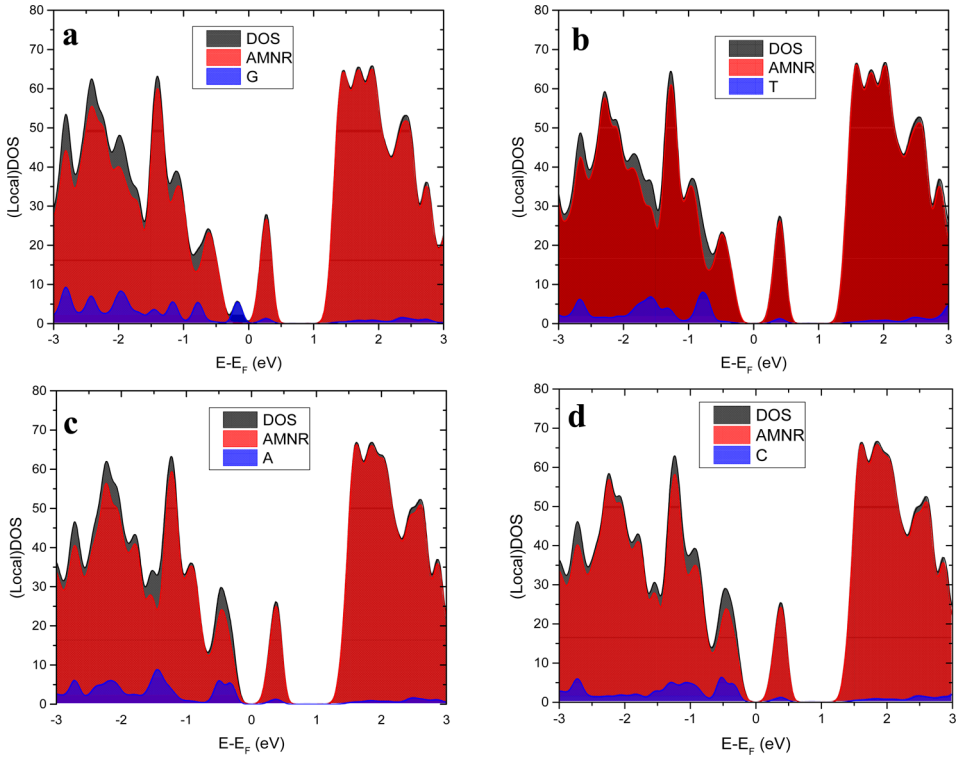

Figure 4. Total and local DOS of a pristine AMNR with each DNA base: (a) guanine (G), (b) thymine (T), (c) adenine (A), and (d) cytosine (C), which is placed on the top of AMNR.

(see Figure 3f). It is noteworthy that bases G and A inherit an additional five-membered ring attached to the six-membered ring compared to bases C and T with only one six-membered ring. The additional ring in bases A and G provides the possibility of sharing a higher level of electronic interactions with MoS_2. To further investigate the origin of the band gap change, the local DOS for pristine AMNR, DNA base, and the total system (base + AMNR) is computed (see Figure 4). The local DOS of AMNR is almost the same for all structures. It should be noted that the band gap change in MoS_2 interacting with base G is mainly due to the overlap of the energy states around the Fermi level induced from base G (Figure 4a). For bases A and C, the finite energy states of each base are located around the Fermi level (Figure 4c,d), unlike the case of base T (Figure 4b), which reduces the band gap.

CONCLUSION

In summary, we found that a single-layer MoS_2 is a promising material for DNA sequencing technology through the nanopore or the surface using MD and DFT simulations. MoS_2 nanopore shows a distinct ionic current signal for single-nucleobase detection with a SNR of 15, which is consistent with the experimental results.[32] MoS_2 also shows a characteristic response in total DOS change for each base. The band gap of MoS_2 is significantly changed when bases are placed on the top of pristine MoS_2, which makes it a good material for base detection. In contrast to graphene, for the MoS_2 nanopore, DNA shows a more distinguishable signature per base. During translocation of DNA, bases stick to the graphene surface while the MoS_2 nanopore shows a nonsticky behavior.

METHODS

MD Simulation. We performed MD simulations with LAMMPS[43] to investigate DNA translocation in a MoS_2 nanopore (Figure 1a). We used the structural features of the hairpin DNA (5′-D (ATCCTA-GTTA-TAGGAT)-3′). The specific feature of this DNA is the formation of a G−A base pair in the loop (Figure 1b). A pore with a diameter of 2.3 nm is drilled in the center of an 8 nm × 8 nm single-layer MoS_2. Initially, DNA was placed at the mouth of the MoS_2 nanopore where the DNA axis (*z*-direction) is along the nanopore axis (Figure 1b). DNA and MoS_2 are submersed in water and salt ionic solution. The ionic concentration of NaCl is 1 M. We used the CHARMM27 force field[44] parameters for DNA, TIP3P water molecules, and ions. SHAKE algorithm was used to maintain the rigidity of the water molecules. The parameters for MoS_2 were taken from ref 45. For the interaction between MoS_2 and DNA, water and ions, we used mixing rules. MoS_2 atoms were frozen to their initial lattice position. In the case of the graphene nanopore, the C−C interaction is modeled with the AIREBO[46] potential. The periodic boundary condition is applied in all three directions. The cutoff distance for the LJ interactions is 15 Å. The long-range electrostatic interactions were computed by using the particle−particle−particle−mesh method. The time step is selected to be 1 fs. For each simulation, energy minimization was performed for 100 000 steps. Systems were then equilibrated for 1 ns with NPT ensemble at 1 atm pressure and 300 K temperature. NPT simulation ensures that the water concentration is equal to the bulk value of 1 g/cm^3. The simulation is then performed in NVT ensemble. Temperature was maintained at 300 K by applying the Nosè−Hoover thermostat with a time constant of 0.1 ps. Before applying the electric field, equilibration for 2 ns is performed in NVT. Production simulations were performed by applying an external electric field in the *z*-direction. The external electric fields are reported in terms of a transmembrane voltage difference $V = EL_z$, where E is the electric field strength and L_z is the length of the simulation system in the *z*-direction.[16] We monitored the time-dependent ionic current, $I(t)$, in the pore. We computed the ionic current through the nanopore by using the definition of current

$$I(t) = \frac{1}{L_z}\sum_{i=1}^{n} q_i\left[\frac{z_i(t+\delta t) - z_i(t)}{\delta t}\right]$$

where the sum is for all the ions, δt is chosen to be 5 ps, and z_i and q_i are the *z*-coordinate, charge of ion *i*, and n is the total number of ions.

DFT Simulation. We performed DFT with SIESTA to understand the physical nature of interaction between MoS_2 and nucleobases.[47] DFT has been widely used to investigate the physical/chemical adsorption mechanism, and it has also been shown that it can accurately capture the electronic properties of nanomaterials, such as MoS_2, water-filled buckyball, and graphene.[26,41,42,48] For parametrization of the exchange-correlation functional, generalized gradient approximation with Perdew−Burke−Ernzerhof is used.[49] The core electrons are replaced by the norm-conserving pseudopotentials.[50] For the basis set, double-ζ basis plus polarization numerical atomic orbital is used. For the *k*-point mesh generation, the 5 × 5 × 1 Monkhorst−Pack for structural relaxation for both MoS_2 and DNA and 12 × 12 × 1 (bulk structure) and 1 × 1 × 40 (finite structure) Monkhorst−Pack for calculation of electronic properties are used.[51] A vacuum region of around 20 Å is used to remove any artificial effect from the nonperiodic directions in the simulation box. Structural relaxation is achieved until the maximum residual force of the system is reached, which is less than 0.05 eV/Å. For MoS_2 structure construction, the unit cell of MoS_2 is first relaxed, and using it, a larger system is generated for interaction with DNA bases (Supporting Information). After energy minimization, the total density of states of the system (MoS_2 + DNA bases), which represents the number of states for each energy level, is obtained. The binding energy between MoS_2 substrate and DNA bases is calculated as $E_{binding} = (E_{MoS_2} + E_{base}) - E_{total}$, where E_{total} is the total energy of the system (MoS_2 and base), and E_{MoS_2} and E_{base} is the energy of each system, MoS_2 and single base, respectively. For the interaction of pristine MoS_2 with DNA base, the band gap change is studied. To understand that the electron clouds overlap due to the interaction between MoS_2 and DNA bases, the charge density difference ($\Delta\rho$) is obtained, which is defined as $\Delta\rho = \rho_{MoS_2+base} - (\rho_{MoS_2} + \rho_{base})$, where $\rho_{MoS_2}$and ρ_{base} represent the charge density distribution of each structure (MoS_2 and DNA base), and ρ_{MoS_2+base} is the charge density distribution of the total system.

Conflict of Interest: The authors declare no competing financial interest.

Acknowledgment. This work is supported by AFOSR under Grant No. FA9550-12-1-0464 and by NSF under Grants 1127480 and 1264282. The authors gratefully acknowledge the use of the parallel computing resource (Taub campus cluster and Blue Waters) provided by the University of Illinois. We acknowledge that Figure 3b is generated using the XCrySDen program.[52] This work used the Extreme Science and Engineering Discovery Environment (XSEDE), which is supported by the National Science Foundation Grant No. OCI-1053575.

Supporting Information Available: Calculation of SNR, water flux through the nanopore, orientation of bases in the nanopore, determination of conduction states, translocation history

of DNA *versus* different biases and electronic DFT calculation of ion effect in the nanopore are available. This material is available free of charge *via* the Internet at http://pubs.acs.org.

REFERENCES AND NOTES

1. Deamer, D. W.; Branton, D. Characterization of Nucleic Acids by Nanopore Analysis. *Acc. Chem. Res.* **2002**, *35*, 817–825.
2. Branton, D.; Deamer, D. W.; Marziali, A.; Bayley, H.; Benner, S. A.; Butler, T.; Di Ventra, M.; Garaj, S.; Hibbs, A.; Huang, X. H.; *et al.* The Potential and Challenges of Nanopore Sequencing. *Nat. Biotechnol.* **2008**, *26*, 1146–1153.
3. Fologea, D.; Gershow, M.; Ledden, B.; McNabb, D. S.; Golovchenko, J. A.; Li, J. L. Detecting Single Stranded DNA with a Solid State Nanopore. *Nano Lett.* **2005**, *5*, 1905–1909.
4. Dekker, C. Solid-State Nanopores. *Nat. Nanotechnol.* **2007**, *2*, 209–215.
5. Aksimentiev, A.; Heng, J. B.; Timp, G.; Schulten, K. Microscopic Kinetics of DNA Translocation through Synthetic Nanopores. *Biophys. J.* **2004**, *87*, 2086–2097.
6. Chen, Z.; Jiang, Y. B.; Dunphy, D. R.; Adams, D. P.; Hodges, C.; Liu, N. G.; Zhang, N.; Xomeritakis, G.; Jin, X. Z.; Aluru, N. R.; *et al.* DNA Translocation through an Array of Kinked Nanopores. *Nat. Mater.* **2010**, *9*, 667–675.
7. Heng, J. B.; Aksimentiev, A.; Ho, C.; Marks, P.; Grinkova, Y. V.; Sligar, S.; Schulten, K.; Timp, G. The Electromechanics of DNA in a Synthetic Nanopore. *Biophys. J.* **2006**, *90*, 1098–1106.
8. Heng, J. B.; Aksimentiev, A.; Ho, C.; Marks, P.; Grinkova, Y. V.; Sligar, S.; Schulten, K.; Timp, G. Stretching DNA Using the Electric Field in a Synthetic Nanopore. *Nano Lett.* **2005**, *5*, 1883–1888.
9. Min, S. K.; Kim, W. Y.; Cho, Y.; Kim, K. S. Fast DNA Sequencing with a Graphene-Based Nanochannel Device. *Nat. Nanotechnol.* **2011**, *6*, 162–165.
10. Venkatesan, B. M.; Bashir, R. Nanopore Sensors for Nucleic Acid Analysis. *Nat. Nanotechnol.* **2011**, *6*, 615–624.
11. Iqbal, S. M.; Akin, D.; Bashir, R. Solid-State Nanopore Channels with DNA Selectivity. *Nat. Nanotechnol.* **2007**, *2*, 243–248.
12. Li, J. L.; Gershow, M.; Stein, D.; Brandin, E.; Golovchenko, J. A. DNA Molecules and Configurations in a Solid-State Nanopore Microscope. *Nat. Mater.* **2003**, *2*, 611–615.
13. Meller, A.; Nivon, L.; Brandin, E.; Golovchenko, J.; Branton, D. Rapid Nanopore Discrimination between Single Polynucleotide Molecules. *Proc. Natl. Acad. Sci. U.S.A.* **2000**, *97*, 1079–1084.
14. Sathe, C.; Zou, X. Q.; Leburton, J. P.; Schulten, K. Computational Investigation of DNA Detection Using Graphene Nanopores. *ACS Nano* **2011**, *5*, 8842–8851.
15. Siwy, Z. S.; Davenport, M. Nanopores Graphene Opens up to DNA. *Nat. Nanotechnol.* **2010**, *5*, 697–698.
16. Wells, D. B.; Belkin, M.; Comer, J.; Aksimentiev, A. Assessing Graphene Nanopores for Sequencing DNA. *Nano Lett.* **2012**, *12*, 4117–4123.
17. Geim, A. K.; Novoselov, K. S. The Rise of Graphene. *Nat. Mater.* **2007**, *6*, 183–191.
18. Nelson, T.; Zhang, B.; Prezhdo, O. V. Detection of Nucleic Acids with Graphene Nanopores: *Ab Initio* Characterization of a Novel Sequencing Device. *Nano Lett.* **2010**, *10*, 3237–3242.
19. Schneider, G. F.; Kowalczyk, S. W.; Calado, V. E.; Pandraud, G.; Zandbergen, H. W.; Vandersypen, L. M. K.; Dekker, C. DNA Translocation through Graphene Nanopores. *Nano Lett.* **2010**, *10*, 3163–3167.
20. Traversi, F.; Raillon, C.; Benameur, S. M.; Liu, K.; Khlybov, S.; Tosun, M.; Krasnozhon, D.; Kis, A.; Radenovic, A. Detecting the Translocation of DNA through a Nanopore Using Graphene Nanoribbons. *Nat. Nanotechnol.* **2013**, *8*, 939–945.
21. Saha, K. K.; Drndic, M.; Nikolic, B. K. DNA Base-Specific Modulation of Microampere Transverse Edge Currents through a Metallic Graphene Nanoribbon with a Nanopore. *Nano Lett.* **2012**, *12*, 50–55.
22. Prasongkit, J.; Grigoriev, A.; Pathak, B.; Ahuja, R.; Scheicher, R. H. Transverse Conductance of DNA Nucleotides in a Graphene Nanogap from First Principles. *Nano Lett.* **2011**, *11*, 1941–1945.
23. Banerjee, S.; Shim, J.; Rivera, J.; Jin, X. Z.; Estrada, D.; Solovyeva, V.; You, X.; Pak, J.; Pop, E.; Aluru, N.; *et al.* Electrochemistry at the Edge of a Single Graphene Layer in a Nanopore. *ACS Nano* **2013**, *7*, 834–843.
24. Tsutsui, M.; Taniguchi, M.; Yokota, K.; Kawai, T. Identifying Single Nucleotides by Tunnelling Current. *Nat. Nanotechnol.* **2010**, *5*, 286–290.
25. Tsutsui, M.; Taniguchi, M.; Kawai, T. Transverse Field Effects on DNA-Sized Particle Dynamics. *Nano Lett.* **2009**, *9*, 1659–1662.
26. Kumar, B.; Min, K.; Bashirzadeh, M.; Farimani, A. B.; Bae, M. H.; Estrada, D.; Kim, Y. D.; Yasaei, P.; Park, Y. D.; Pop, E.; Aluru, N. R.; *et al.* The Role of External Defects in Chemical Sensing of Graphene Field-Effect Transistors. *Nano Lett.* **2013**, *13*, 1962–1968.
27. Obradovic, B.; Kotlyar, R.; Heinz, F.; Matagne, P.; Rakshit, T.; Giles, M. D.; Stettler, M. A.; Nikonov, D. E. Analysis of Graphene Nanoribbons as a Channel Material for Field-Effect Transistors. *Appl. Phys. Lett.* **2006**, *88*, 142102.
28. Radisavljevic, B.; Radenovic, A.; Brivio, J.; Giacometti, V.; Kis, A. Single-Layer MoS_2 Transistors. *Nat. Nanotechnol.* **2011**, *6*, 147–150.
29. Li, J. P.; Zhang, Y.; Yang, J. K.; Bi, K. D.; Ni, Z. H.; Li, D. Y.; Chen, Y. F. Molecular Dynamics Study of DNA Translocation through Graphene Nanopores. *Phys. Rev. E* **2013**, *87*, 062707.
30. Lv, W. P.; Chen, M. D.; Wu, R. A. The Impact of the Number of Layers of a Graphene Nanopore on DNA Translocation. *Soft Matter* **2013**, *9*, 960–966.
31. Paik, K. H.; Liu, Y.; Tabard-Cossa, V.; Waugh, M. J.; Huber, D. E.; Provine, J.; Howe, R. T.; Dutton, R. W.; Davis, R. W. Control of DNA Capture by Nanofluidic Transistors. *ACS Nano* **2012**, *6*, 6767–6775.
32. Liu, K.; Feng, J. D.; Kis, A.; Radenovic, A. Atomically Thin Molybdenum Disulfide Nanopores with High Sensitivity for DNA Translocation. *ACS Nano* **2014**, *8*, 2504–2511.
33. Smeets, R. M. M.; Keyser, U. F.; Dekker, N. H.; Dekker, C. Noise in Solid-State Nanopores. *Proc. Natl. Acad. Sci. U.S.A.* **2008**, *105*, 417–421.
34. Cracknell, J. A.; Japrung, D.; Bayley, H. Translocating Kilobase RNA through the Staphylococcal α-Hemolysin Nanopore. *Nano Lett.* **2013**, *13*, 2500–2505.
35. Lu, B.; Albertorio, F.; Hoogerheide, D. P.; Golovchenko, J. A. Origins and Consequences of Velocity Fluctuations during DNA Passage through a Nanopore. *Biophys. J.* **2011**, *101*, 70–79.
36. Li, Z.; Chen, Y.; Li, X.; Kamins, T. I.; Nauka, K.; Williams, R. S. Sequence-Specific Label-Free DNA Sensors Based on Silicon Nanowires. *Nano Lett.* **2004**, *4*, 245–247.
37. Fritz, J.; Cooper, E. B.; Gaudet, S.; Sorger, P. K.; Manalis, S. R. Electronic Detection of DNA by Its Intrinsic Molecular Charge. *Proc. Natl. Acad. Sci. U.S.A.* **2002**, *99*, 14142–14146.
38. Zhou, Y.; Yang, P.; Zu, H.; Gao, F.; Zu, X. Electronic Structures and Magnetic Properties of MoS_2 Nanostructures: Atomic Defect, Nanohole, Nanodot and Antidot. *Phys. Chem. Chem. Phys.* **2013**, *15*, 10385–10394.
39. Kou, L.; Tang, C.; Zhang, Y.; Heine, T.; Chen, C.; Frauenheim, T. Tuning Magnetism and Electronic Phase Transitions by Strain and Electric Field in Zigzag MoS_2 Nanoribbons. *J. Phys. Chem. Lett.* **2012**, *3*, 2934–2941.
40. Dolui, K.; Pemmaraju, C. D.; Sanvito, S. Electric Field Effects on Armchair MoS_2 Nanoribbons. *ACS Nano* **2012**, *6*, 4823–4834.
41. Lee, J.-H.; Choi, Y.-K.; Kim, H.-J.; Scheicher, R. H.; Cho, J. H. Physisorption of DNA Nucleobases on h-BN and Graphene: vdW-Corrected DFT Calculations. *J. Phys. Chem. C* **2013**, *117*, 13435–13441.
42. Le, D.; Kara, A.; Schröder, E.; Hyldgaard, P.; Rahman, T. S. Physisorption of Nucleobases on Graphene: A Comparative van der Waals Study. *J. Phys.: Condens. Matter* **2012**, *24*, 424210.

43. Plimpton, S. Fast Parallel Algorithms for Short-Range Molecular-Dynamics. *J. Comput. Phys.* **1995**, *117*, 1–19.
44. MacKerell, A. D.; Banavali, N. K. All-Atom Empirical Force Field for Nucleic Acids: II. Application to Molecular Dynamics Simulations of DNA and RNA in Solution. *J. Comput. Chem.* **2000**, *21*, 105–120.
45. Stewart, J. A.; Spearot, D. E. Atomistic Simulations of Nanoindentation on the Basal Plane of Crystalline Molybdenum Disulfide (MoS_2). *Modell. Simul. Mater. Sci. Eng.* **2013**, *21*, 045003.
46. Stuart, S. J.; Tutein, A. B.; Harrison, J. A. A Reactive Potential for Hydrocarbons with Intermolecular Interactions. *J. Chem. Phys.* **2000**, *112*, 6472–6486.
47. Soler, J. M.; Artacho, E.; Gale, J. D.; García, A.; Junquera, J.; Ordejón, P.; Sánchez-Portal, D. The SIESTA Method for *Ab Initio* Order-N Materials Simulation. *J. Phys.: Condens. Matter* **2002**, *14*, 2745.
48. Min, K.; Farimani, A. B.; Aluru, N. Mechanical Behavior of Water Filled C60. *Appl. Phys. Lett.* **2013**, *103*, 263112.
49. Perdew, J. P.; Burke, K.; Ernzerhof, M. Generalized Gradient Approximation Made Simple. *Phys. Rev. Lett.* **1996**, *77*, 3865–3868.
50. Troullier, N.; Martins, J. L. Efficient Pseudopotentials for Plane-Wave Calculations. *Phys. Rev. B* **1991**, *43*, 1993–2006.
51. Monkhorst, H. J.; Pack, J. D. Special Points for Brillouin-Zone Integrations. *Phys. Rev. B* **1976**, *13*, 5188–5192.
52. Kokalj, A. Computer Graphics and Graphical User Interfaces as Tools in Simulations of Matter at the Atomic Scale. *Comput. Mater. Sci.* **2003**, *28*, 155–168.